Quirce, A., et al. Polarization dynamics in VCSEL-based gain switching optical frequency combs. In: *Journal of Lightwave Technology, 36(10), May 2018, pp. 1798-1806*

DOI: 10.1109/JLT.2018.2790435

Polarization Dynamics in VCSEL-Based Gain Switching Optical Frequency Combs

Ana Quirce, Cristina de Dios, Angel Valle, Luis Pesquera, and Pablo Acedo, Member, IEEE

***Abstract*—In this paper, we report on the polarization dynamics of a 1550 nm vertical-cavity surface-emitting laser (VCSEL) under gain switching regime. We focus our analysis on the resulting optical frequency combs associated with the main and suppressed polarization modes. Measurement of the parameters characterizing the polarization behavior of our single-transverse mode VCSEL is performed from the analysis of high-resolution optical spectra. An extension of the spin-flip rate model to include nonlinear carrier recombination is developed. An analysis of polarization-resolved dynamics is performed by using the previous model with the measured VCSEL parameters. We show that two orthogonally polarized combs are generated that combine to produce a wider overall optical comb. We analyze the dependence of combs on the amplitude and frequency of the modulation. Our results are in agreement with experiments reported by Prior *et al.* We also analyze the dependence of the combs on the linear dichroism of the VCSEL We show that the change of this dichroism results in bistability between the two orthogonally polarized combs.**

***Index Terms*—Gain switching, optical frequency comb generator, semiconductor lasers, vertical-cavity surface-emitting lasers.**

I. Introduction

GENERATION of Optical frequency combs (OFCs) has recently become a major research topic [1]. They are versatile systems that have found application in disciplines such as spectroscopy [2], [3], THz generation [4] or optical communications [5].

Among the available technologies for the generation of OFCs, compact systems are interesting to decrease the cost, energy consumption and complexity. Such optical frequency combs would contribute to take out of the laboratory technologies such as dual-combs [3] or optical processing [6].

In this sense, OFCs based on laser diodes (LDs) using Gain Switching (GS) techniques offer suitable combs with competitive costs and efficiency [7]. Gain-switching consists on the large signal modulation of the current applied to a semiconductor laser to produce a regular pulse train. This technique offers good tunability characteristics, low cost, compactness and high correlation between optical modes. It can be implemented using typical commercial semiconductor lasers. For instance Vertical-Cavity Surface-Emitting Lasers (VCSEL) [8] are appealing for this comb generation because they can take this advantage even further because of their low cost, compactness, and low energy consumption, opening the possibility of mass production [9].

VCSELs have several advantages compared to edge emitting semiconductor lasers [10], [11], for instance, on-wafer testing capability, reduced manufacturing costs, low energy consumption, ease of fabrication of 2 dimensional arrays, and circular output beam [10], [11]. VCSELs emit in a single-longitudinal mode but they can emit in a single or multiple transverse modes. Emission in two linear polarization modes with orthogonal directions can be found in such a way that changes in the temperature or current can produce polarization switching (PS) between these two modes [12]–[15].

Extraction of the working parameters of the VCSEL is important for a realistic theoretical description of VCSEL-based gain switching optical frequency combs (VGSOFC). Parameter extraction in VCSELs have mainly focused on single-polarization mode devices [16]–[21]. However, the important role played by polarization dynamics in VGSOFC [7] suggests that parameters characterizing the polarization properties of the device must be extracted for a good theoretical description of the system. Different procedures for polarization-resolved characterization of VCSEL parameters have been developed [22]–[25]. Devices in [22]–[25] are characterized by a different technology to that of VCSELs used in GSOFC experiments [7]. In this way an specific characterization of devices used in [7] is of interest for VGSOFC modelling and for comparison of parameters of long-wavelength VCSELs obtained by using different technologies.

Theoretical analysis of polarization properties of VCSELs is usually performed by using the spin-flip model (SFM) [12] in which carrier linear recombination is assumed. However, if the device is gain-switched with large values of the amplitude of the bias current there are large variations of carriers. Under these circumstances, the usual linearization of carrier recombination rate in rate equations could not be a good approximation. Nonlinear carrier recombination seems more appropriated to describe optical frequency combs from gain-switched

Manuscript received October 31, 2017; revised December 28, 2017; accepted January 3, 2018. This work was supported by the Ministerio de Economía y Competitividad (MINECO/FEDER, UE), Spain, under projects TEC2015-65212-C3-1-P and TEC2014-52147-R. The work of A. Quirce was supported by the Fonds Wetenschappelijk for the Post-Doctoral Fellowship. The work of
K. Panajotov was supported by the Methusalem foundation. *(Corresponding author: Angel Valle.)*

A. Quirce is with the Faculty of Engineering Sciences, Vrije Universiteit Brussel, Brussels 1050, Belgium (e-mail: aquirce@b-phot.org).

C. de Dios and P. Acedo are with the Universidad Carlos III de Madrid, Madrid 28911, Spain (e-mail: cdios@ing.uc3m.es; pag@ing.uc3m.es).

A. Valle and L. Pesquera are with the Instituto de Física de Cantabria, Santander E39005, Spain (e-mail: valle@ifca.unican.es; pesquerl@ifca.unican.es).

semiconductor lasers [26]. Therefore an extension of the SFM model to include this nonlinearity seems desirable.

In this work we analyze the polarization-resolved optical frequency combs generated by a 1550 nm VCSEL under gain switching modulation. This analysis is done in three steps. First, we measure the parameters that characterize the polarization behavior of our VCSEL. Second, we extend the spin-flip rate model to include nonlinear carrier recombination. In the third step we use this model together with the measured parameters in order to theoretically analyze the characteristics of the generated frequency combs. We show that the orthogonally polarized combs combine to produce a wider overall optical comb. We obtain that the dependence of combs on the amplitude and frequency of the modulation is similar to that experimentally reported in [7]. We interpret our results in terms of optical power and carrier dynamics. Finally we show that bistability between the two orthogonally polarized combs can be found for specific values of the device linear dichroism.

The structure of this paper is organized as follows. We present in Section II the measurement of VCSEL parameters. The theoretical model is described in Section III. Section IV is devoted to describe our results on polarization-resolved optical frequency combs. In Section V we will discuss and summarize our results.

II. Measurement of VCSEL Parameters

In this section we characterize a VCSEL diode laser (VERTILAS VL-1550-8G-P2-H4) provided together with a specific board for radiofrequency (RF) operation within the laser bandwidth. We will mainly follow the techniques developed in [21], [22] in which a different long-wavelength commercial VCSEL (Raycan co.) was characterized. The VERTILAS device under CW operation exhibits a stable emission without any polarization switching in the whole bias current range. The CW optical spectrum at a bias current of 11.5 mA and 20 °C is shown in [7]. The device emits in a single-transverse mode with a dominant linear polarization mode that appears at $\lambda_y = 1537.95$ nm and a residual orthogonal mode emitting at $\lambda_x = 1538.20$ nm[7]. We will follow the notation of [22] in which the x (y) linear polarization has the smallest (largest) optical frequency.

Our characterization techniques are based on measurements of continuous wave optical spectra with 10 MHz frequency resolution. These are obtained with the BOSA optical spectrum analyzer based on stimulated Brillouin scattering [17]. First, we measure with the BOSA the optical power around the lasing frequency, P_w, as a function of the bias current I using a 10 GHz span [21]. The linear fit for bias currents above threshold gives $P_w = 0.1148$ mW/mA $(I - 2.62$ mA) with an adjusted R-square merit value, $\bar{R}^2 = 0.9996$. This fit gives an scale factor between P_w and the current above threshold of $F = 8.71 \pm 0.05$ mA/mW and a first estimation of the threshold current $I_{th} = 2.62 \pm 0.04$ mA. Fitting the values of FP_w as a function of I to [21, eq. (10)] gives the following combination of parameters $\frac{e^2 R_{sp}^{th}}{\tau_n \tau_p G_N} = (1.7 \pm 0.3)10^{-4}$ mA^2 ($\bar{R}^2 = 0.95$) where e is the electron charge and the meaning of the other symbols is shown in Table I.

TABLE I
Parameter Values for the Model of [21]

Parameter	Meaning	Value
G_N	*Differential gain*	$(3.37 \pm 0.09) \cdot 10^4 \mathrm{s}^{-1}$
τ_n	*Differential carrier lifetime at threshold*	0.36 ± 0.04 ns
τ_e	*Carrier lifetime at threshold*	1.05 ± 0.02 ns
τ_p	*Photon lifetime*	14 ± 1 ps
α	*Linewidth enhancement factor*	2.1 ± 0.3
R_{sp}^{th}	*Spontaneous emission rate at threshold*	$(1.0 \pm 0.2) \cdot 10^{12} \mathrm{s}^{-1}$
N_t	*Carrier number at transparency*	$(1.49 \pm 0.03) \cdot 10^7$
N_{th}	*Carrier number at threshold*	$(1.70 \pm 0.03) \cdot 10^7$
I_{th}	*Threshold current*	2.596 ± 0.001 mA
A	*Nonradiative coefficient*	$2.1 \cdot 10^7$ s^{-1}
B	*Radiative coefficient*	$0.9 \cdot 10^{-10}$ cm^{3}s^{-1}
C	*Auger coefficient*	$(1.5 \pm 0.2) \cdot 10^{-29}$ cm^{6}s^{-1}

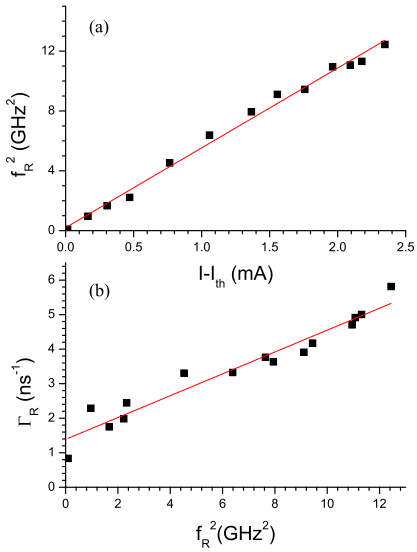

Fig. 1. (a) Squared relaxation oscillation frequencies as a function of $I - I_{th}$. (b) Damping rate of relaxation oscillations as a function of the squared relaxation oscillation frequency. Linear fits are plotted with solid lines.

The differential gain is extracted from measured intensity noise spectra. These are obtained by using an amplified photodetector with 9.5 GHz bandwidth and a 20 GHz microwave spectrum analyzer. Substraction of photodetector and RF analyzer's noise floor and smoothing of the spectrum is done as in [21]. We find the frequency at which the maximum of the noise spectra appears, that approximately corresponds to the relaxation oscillation frequency, f_R. We show in Fig. 1(a) the values of f_R^2 as a function of $I - I_{th}$ and the corresponding linear fit. This fit has a slope of 5.33 ± 0.14 GHz^2/mA and $\bar{R}^2 = 0.992$. Using this slope and [21, eq. (17)] we obtain $G_N = (3.37 \pm 0.09) \cdot 10^4$ s^{-1}.

We measure optical spectra close to threshold in order to obtain the laser linewidth (see [21] for more details). This linewidth is plotted in Fig. 2(a) as a function of $\mid I - I_{th} \mid$ for bias current below threshold. We obtain a linear relation, as predicted in [21]. The slope of this line is $\tau_n G_N/(2\pi e)$ [21]. Since our linear fit has a slope of $(1.06 \pm 0.06) \cdot 10^4$ MHz/mA ($\bar{R}^2 = 0.99$) we get $\tau_n = (0.32 \pm 0.02)$ ns. From the values of τ_n, G_N, and $\frac{e^2 R_{sp}^{th}}{\tau_n \tau_p G_N}$ we get that $R_{sp}^{th}/\tau_p =$

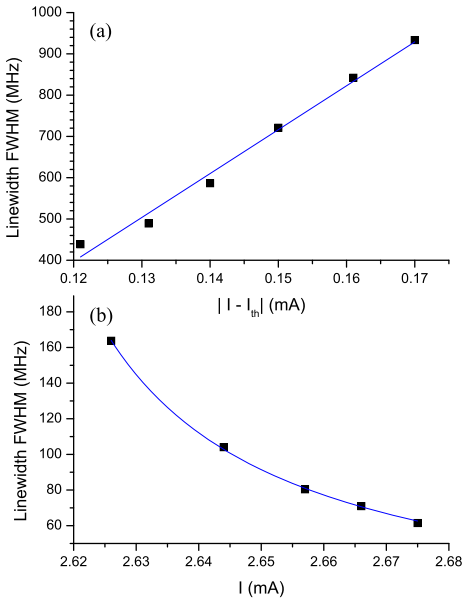

Fig. 2. Width of the Lorentzian component of the laser lineshape as (a) a function of $|\ I - I_{th}\ |$ for bias current below threshold and (b) a function of I for bias current slightly above threshold. Corresponding fits are plotted with solid lines.

$(7.2 \pm 1.4) \cdot 10^{22}$ s^{-2}. The value of the laser linewidth for bias currents slightly above threshold, shown in Fig. 2(b), can be used to obtain the linewidth enhancement factor, α. In this case the laser linewidth is $\Delta\nu_{>} = A_{>}/(I - I_{th})$ where $A_{>} = (1+\alpha^2)eR_{sp}^{th}/(4\pi\tau_p)$ [21]. A two-parameters fit to the previous relation gives the values $A_{>} = 4.96 \pm 0.06$ MHz mA and $I_{th} = 2.596 \pm 0.001$ mA ($\bar{R}^2 = 0.9994$). Linewidth enhancement factor can be obtained from the previous expression of $A_{>}$ and the value of R_{sp}^{th}/τ_p. In this way we obtain $\alpha = 2.1 \pm 0.3$.

The value of the relaxation oscillations damping rate, Γ_R, is obtained from a three-parameters fit of the amplitude noise power spectrum (see [21, eq. (19)]). A linear relation between Γ_R and I is obtained. However the relation between Γ_R and f_R^2

$$\Gamma_R = \frac{1}{2\tau_n} + 2\pi^2 \tau_p' f_R^2 \tag{1}$$

is commonly used in order to extract τ_n and a first estimation of the photon lifetime, τ_p' [27]. We show in Fig. 1(b) the measured relation between Γ_R and f_R^2. We find the following linear relation $\Gamma_R = 1.386\ \text{ns}^{-1} + 0.316\ \text{ns} f_R^2$ ($\bar{R}^2 = 0.94$). Comparison between this relation and (1) gives $\tau_n = (0.36 \pm 0.04)$ ns and $\tau_p' = (16 \pm 1)$ ps. This value of τ_n is consistent with that obtained using Fig. 2(a). The value of τ_p' is obtained without considering gain saturation effects [27]. If this saturation is taken into account we get $\tau_p = \tau_p' - \Gamma\epsilon/(G_N V_a)$ [18], where Γ is the longitudinal confinement factor, ϵ is the gain compression factor, and V_a is the volume of the active region. Using typical values for Vertilas VCSELs with 5 quantum-wells of 8 nm width and 10 μm diameter [28], we get $V_a = 3.14 \cdot 10^{-12}$ cm^3, $\Gamma = 0.05$, $\epsilon = 4.1 \cdot 10^{-18}$ cm^{-3}[18], and $\tau_p = (14 \pm 1)$ ps. Using τ_p and the value for R_{sp}^{th}/τ_p we get $R_{sp}^{th} = (1.0 \pm 0.2) \cdot 10^{11}$ s^{-1}.

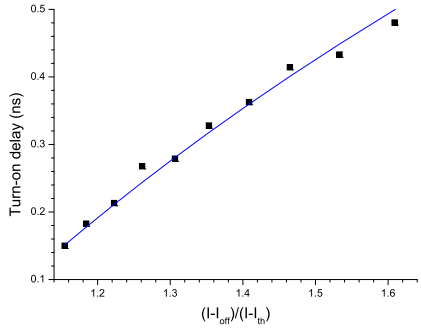

Fig. 3. Turn-on delay of the VCSEL as a function of $(I - I_{\text{off}})/(I - I_{th})$ (symbols) and the fitted theoretical curve with $\tau_e = 1.05$ ns (line).

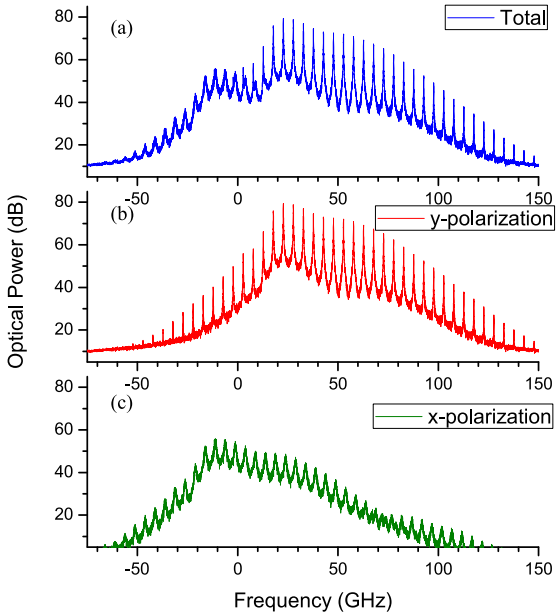

Fig. 4. Simulated optical spectra of (a) the total output, (b) y-polarization mode, and (c) x-polarization mode for $I_0 = 11.5$ mA, $m = 1.3$ and $f_m = 5$ GHz.

Carrier lifetime at threshold, τ_e, can be determined by the measurement of the turn-on delay, t_d, that is the time between switching on the laser current and the reaction of the optical emission [19], [20], [29]. This delay is given by

$$t_d = \tau_e \ln \frac{I - I_{\text{off}}}{I - I_{th}} \tag{2}$$

where the VCSEL is switched from a current below threshold, I_{off}, to a current above threshold, I. We use a bit pattern generator with 30 ps risetime and the light is detected with the high-speed photodetector connected to a real time high-speed (12 GHz) oscilloscope. The current I_{off} is applied during 18 ns because (2) is valid only if the laser is in a stationary state before it is switched on. Fig. 3 shows the measured value of t_d as a function of $(I - I_{\text{off}})/(I - I_{th})$. We have followed the experimental procedure explained in [19] in order to measure the delay. This value has been averaged over 20 consecutive pulses for each value of $(I - I_{\text{off}})/(I - I_{th})$. Fig. 3 also shows with a solid line the fit of the measured values to (2) that yields a carrier lifetime at threshold of $\tau_e = 1.05 \pm 0.02$ ns.

Values of the number of carriers at threshold, N_{th}, and at transparency, N_t, can be found as follows. We use $N_{th} = \tau_e I_{th}/e$ [21] to obtain that $N_{th} = (1.70 \pm 0.03) \cdot 10^7$. We also use $N_t = N_{th} - 1/(G_N \tau_p)$ [21] to get $N_t = (1.49 \pm 0.03) \cdot 10^7$. The values of the coefficients A, B, and C that determine the carrier recombination rate are obtained in the following way. We take the values for the nonradiative recombination coefficient, $A = 2.1 \cdot 10^7$ s^{-1}, and for the radiative recombination coefficient, $B = 0.9 \cdot 10^{-10}$ cm^{3}s^{-1} given in [18]. The range of variation of B for long-wavelength VCSELs is small [18], [20], [30]. However the range of variation of A for these devices is wider but its value has a small impact on the determination of the turn-on delay [30]. The value of the Auger recombination coefficient, C, for our VCSEL is obtained as follows. Using [21, eq. (20)] and $I_{th} = N_{th} e/\tau_e$ we get $C = \left(\frac{1}{\tau_e} - A\right)\left(\frac{V_a}{N_{th}}\right)^2 - B\frac{V_a}{N_{th}}$ that gives $C = (1.5 \pm 0.2) \cdot 10^{-29}$ cm^{6}s^{-1}, very close to that found in [18]. A summary of the obtained parameters is given in Table I.

III. Theoretical Model

We perform the theoretical study of the optical frequency comb generation in VCSELs by using the spin-flip model (SFM) [31], [32]. This model describes the dynamical evolution of the linear polarization modes of a VCSEL emitting in its fundamental transverse mode. In this way we can analyze each of the two linearly polarized combs generated in this device. A linear expansion of the carrier recombination rate around the number of carriers at threshold is usually assumed for obtaining the model equations (see (7)–(10) in the Appendix) [21], [22]. However, conditions for obtaining gain-switched optical frequency combs are such that the modulation index, m, is large and the difference between the number of carriers and its value at threshold can become large as well. In this way the previous linearizacion could be no longer valid and consideration of nonlinear carrier recombination would seem desirable in order to have a more realistic description of frequency combs dynamics. In order to do this we depart from the equation for the carrier number, N, in a linearly polarized single-mode laser diode with nonlinear recombination rate [21]

$$\frac{dN}{dt} = \frac{I}{e} - \left(AN + \frac{B}{V_a}N^2 + \frac{C}{V_a^2}N^3\right) - G_N(N - N_t)P \tag{3}$$

When considering the change of variables [22] $D = (N - N_t)/(N_{th} - N_t)$ and $P' = G_N \tau_n P$ we get

$$\frac{dD}{dt} = \frac{I}{e\Delta N_t} - \mathbb{R}\,(D) - \gamma D P' \tag{4}$$

where

$$\mathbb{R}(D) = A\Big(D + D_t\Big) + \mathbb{B}\Big(D + D_t\Big)^2 + \mathbb{C}\Big(D + D_t\Big)^3, \tag{5}$$

$\Delta N_t = N_{th} - N_t$, $D_t = N_t/\Delta N_t$, $\mathbb{B} = B\Delta N_t/V_a$, and $\mathbb{C} = C\Delta N_t^2/V_a^2$. The extension to the case of a VCSEL with two linear polarizations can be done as in [22] by substituting (9) by the following equation in order to consider nonlinear recombination

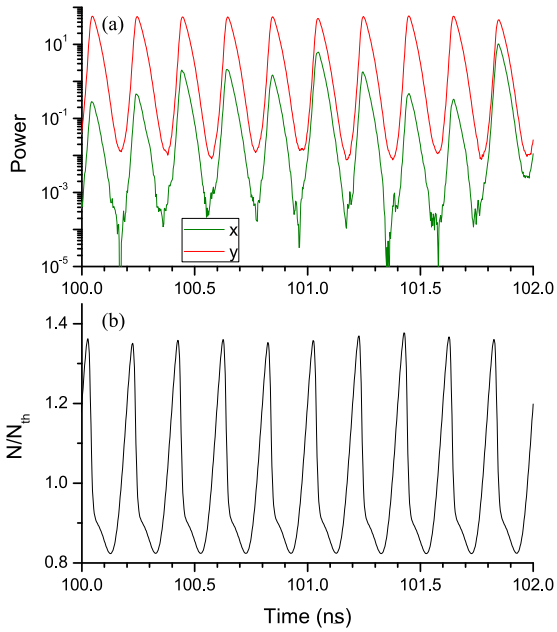

Fig. 5. (a) Simulated time traces of the power of x (green line) and y-polarization (red line) modes, (b) Simulated time trace of the ratio between the carrier number and carrier number at threshold. $I_0 = 11.5$ mA, $m = 1.3$ and $f_m = 5$ GHz.

$$\frac{dD}{dt} = \frac{I}{e\Delta N_t} - \mathbb{R}(D) - \gamma[D(|E_x|^2 + |E_y|^2) + in(E_y E_x^* - E_x E_y^*)] \tag{6}$$

We can check that (9) and (6) are consistent by linearizing (6) around $D = 1$, that corresponds to linearizing around the threshold value. In fact, using the linear expansion of $\mathbb{R}$, $\mathbb{R}(D) \approx \mathbb{R}(1) + \gamma(D - 1)$ in (6) and applying $\mathbb{R}(1) = I_{th}/(e\Delta N_t)$ we get (9) and (11).

We consider that the bias current depends sinusoidally on time in the following way, $I(t) = I_0(1 + m\cos(2\pi f_m t))$ in order to simulate frequency combs generation by gain switching the VCSEL. In this expression I_0 is the applied bias current, m is the modulation index and f_m is the modulation frequency. We note that the total current can be negative when $m > 1$. Negative currents are also obtained when the voltage across a diode is switched from the forward direction to the reverse (see [33, Sec. 2.5] and [34]). Negative currents have also been used to model pulse generation in VCSELs in [35]. We have checked that in all the simulations a positive value for the carrier number is obtained [see Fig. 5(b) for $m = 1.3$]. Moreover we obtain qualitatively similar results when using the same current but with the negative values substituted by a zero current value.

The linear birefringence parameter, γ_p, is measured from the frequency splitting between the y and the x polarizations, $\nu_y - \nu_x$ (32.88 GHz) in the following way, $\gamma_p = \pi(\nu_y - \nu_x) + \alpha\gamma_a$ [31]. The linear dichroism is obtained from the difference between the spectral widths of the two linear polarizations [22]. We have measured this parameter as in [22], from $I = 3$ to $I = 8$ mA, and we have obtained values that depend on I, as in [22]. γ_a is positive as the x-polarization mode is suppressed. It

TABLE II
VCSEL'S PARAMETER VALUES FOR OUR MODEL

Parameter	Meaning	Value
κ	*Field decay rate*	36 ± 3 ns^{-1}
γ_a	*Linear dichroism*	1.4 ± 0.5 ns^{-1}
γ_p	*Linear birefringence*	$106\pm$ 1 ns^{-1}
γ	*Decay rate of D*	2.8 ± 0.3 ns^{-1}
γ_s	*Spin-flip relaxation rate*	1000 ns^{-1}
β_{SF}	*Spontaneous emission parameter*	$(5.4 \pm 1.7) \cdot 10^{-4}$
$\mathbb{B}$	Scaled radiative coefficient	$(6.0 \pm 1.2) \cdot 10^{7}$ s^{-1}
$\mathbb{C}$	Scaled Auger coefficient	$(7 \pm 3) \cdot 10^{6}$ s^{-1}

has a local maximum (1.9 ns^{-1}) and a local minimum (0.9 ns^{-1}) at 4 and 6 mA, respectively. In our calculations we will take an effective value for γ_a given by the average of the measured values with an uncertainty given by its maximum excursions $\gamma_a = 1.4 \pm 0.5$ ns^{-1}. The method we followed to measure the spin flip rate, γ_s, in [22] can not be applied in our device because it is based on observation of polarization switching, that does not appear in our laser. Values of γ_s reported in the literature for long-wavelength VCSELs are large, 620 ns^{-1} [25], 1000 ns^{-1} [24], 2100 ns^{-1} [22]. We will take an intermediate value $\gamma_s = 1000$ ns^{-1}. Although γ_s is large we have preferred to maintain the complete model for knowing the range of γ_s for which we get similar results. Also the model can be used for other VCSELs in which spin effects are important. Our simulations of the model indicate that results are similar if $\gamma_s >$ 300 ns^{-1}. For these values of γ_s, n is small in such a way that there is no important effects on the dynamics. The numerical values of the model parameters are given in Table II. The remaining parameters can be found in Table I.

IV. THEORETICAL RESULTS

We numerically integrate the model with nonlinear carrier recombination, (6), (7), (8), and (10) in order to obtain the optical spectra. These spectra are calculated using a 0.01 ps integration time step, a 2.5 ps sampling time, and an average over twenty different time windows of 40.96 ns duration. Optical spectra corresponding to the total power and both linear polarizations are shown in Fig. 4 for $I_0 = 11.5$ mA, $m = 1.3$ and $f_m = 5$ GHz. I_0, f_m and frequency span are similar to those in [7, Fig. 5]. m has been chosen to get similar ratios in experiment and theory between the maximum of the total output spectrum spectrum and the local maximum close to -10 GHz [see Fig. 4(a), around 25 dB]. Comparison between Figs. 4 and [7, Fig. 5] shows that good qualitative agreement is found between experimental and theoretical results. We note that our y-polarization mode corresponds to the x-polarization mode in [7] because both are the dominating modes that appear at large optical frequencies. Comb lines are better defined in theoretical results because the frequency separation between consecutive points in the spectrum, 24.4 MHz, is much smaller than the frequency resolution of the optical spectrum analyzer, 3 GHz, in [7]. Fig. 4 shows that the total output comb has two main contributions due to each of the linearly polarized combs. The x-polarization mode exhibits an optical comb with lower optical power and smaller central frequency. The frequency separation between the maximum of each subcomb is 33.9 GHz, close to the frequency splitting between the polarization modes under CW operation. Like in [7] the ratio between the maximum of y and x-polarized combs, 25 dB, is much smaller than the polarization mode suppression ratio obtained at CW operation (38 dB). This indicates that gain-switching regime enhances the power associated to the suppressed polarized signal, in agreement with [7].

The time evolution of the power of both linear polarizations is shown in Fig. 5(a) for the same conditions of Fig. 4. A vertical logarithmic scale has been chosen in order to show also the effect of spontaneous emission noise. A regular pulse train with 5 GHz repetition frequency is observed for the y-polarization. Pulse minima are well above the level at which spontaneous emission noise dominates the evolution (10^{-4}). A pulse train is also observed for the x-polarization at the same repetition frequency. However a great dispersion in the maximum of the pulses appears due to the large effect of spontaneous emission noise on the dynamics of the $x-$polarized mode. The maximum values of the pulses for the x-polarization in Fig. 5(a) vary in the range from 0.3 to 10.3. The minimum values of these pulses vary in the range from 10^{-6} to 2×10^{-3}. Then the standard deviation of the maximum of the pulses (3.2) is greater than that of the minimum (8×10^{-4}). Power of the x-polarized mode is much smaller than that of the other mode and almost all the pulses have minima at the noise level. Some spontaneous emission noise events can happen in such a way that x and $y-$polarized pulses have maximum in the same order of magnitude [see the last pulse in Fig. 5(a)]. Fig. 5(b) shows the evolution of the ratio between the carrier number and the carrier number at threshold, $N(t)/N_{th}$. It shows, together with Fig. 5(a), typical formation of pulses by gain switching.

In [7] the number of modes exhibited by the combs has been measured when the amount of radiofrequency (RF) power injected to modulate the laser and the modulation frequency change (see [7, Fig. 4]). The broadest comb is obtained in experiments for a bias current of 11.5 mA when the RF power is 16 dBm and the RF frequency is 5 GHz. We now discuss the effect of changing the modulation frequency and the modulation index on the dynamics of the system. We analyze two characteristics of the comb: the number of modes, N_{mod}, that is evaluated considering 10 dB optical bandwidth for the total power, and the teeth depth, TD, defined as the difference between the maximum of the optical spectrum and the minimum of its next valley. Figs. 6 and 7 show optical spectra and their corresponding time traces of the power of both linear polarizations and total power for different values of f_m and m. Figs. 6(a) and 7(a) show the effect of decreasing the value of f_m with respect to that considered in Fig. 4. Comparison between Figs. 4(a) and 6(a) shows that teeth in optical frequency combs for the total and linearly polarized powers almost dissappear when f_m decreases to 3 GHz. In this case, Fig. 7(a) shows that power of both linear polarizations, and so the total power, decrease to small values in which spontaneous emission noise dominates the evolution in such a way that the phase coherence between pulses disappears and frequency combs are degraded. Minimum powers in Fig. 7(a) are smaller than those for the dominant polarization in Fig. 5(a). The minimum values of the pulses for

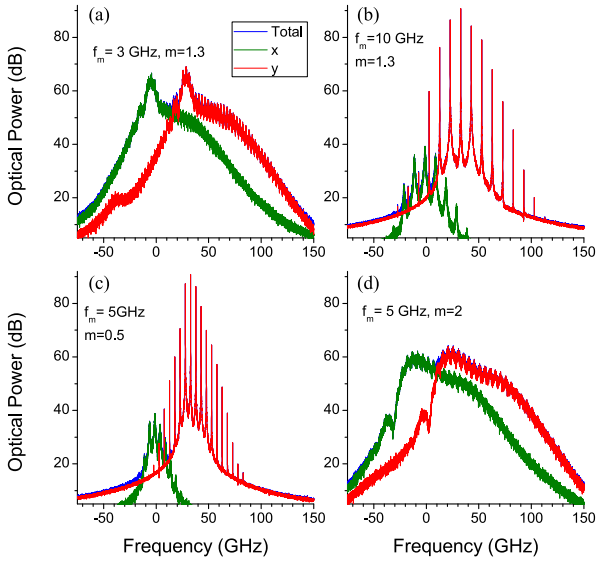

Fig. 6. Simulated optical spectra of the total output, x-polarization , and y-polariation modes for (a) $f_m = 3$ GHz, $m = 1.3$ (b) $f_m = 10$ GHz, $m = 1.3$ (c) $f_m = 5$ GHz, $m = 0.5$, and (d) $f_m = 5$ GHz, $m = 2$. The bias current is $I_0 = 11.5$ mA.

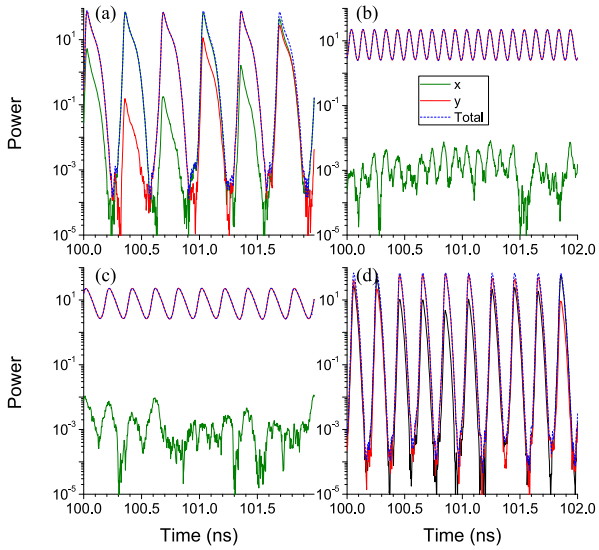

Fig. 7. Simulated time traces of the power of x (green line) and y-polarization (red line) modes. The total power is plotted with blue dashed line. Conditions are similar to those of Fig. 6: (a) $f_m = 3$ GHz, $m = 1.3$ (b) $f_m = 10$ GHz, $m = 1.3$ (c) $f_m = 5$ GHz, $m = 0.5$, and (d) $f_m = 5$ GHz, $m = 2$. The bias current is $I_0 = 11.5$ mA.

both linear polarizations and total power in Fig. 7(a) are less than 10^{-3}. However, the minimum values of the pulses for the y-polarization in Fig. 5(a) are greater than 8×10^{-3}. Fig. 7(a) shows that pulses in both polarizations fluctuate in such a way that the total power remains regularly pulsing with pulses of similar heights. This corresponds to the typical mode partition noise phenomenon observed in semiconductor lasers, like for instance in the longitudinal modes of a DFB laser [36] or in the polarization modes of a VCSEL[37]. Fig. 7(a) shows that a clear anticorrelation between polarization modes is observed, similar to that observed in [36], [37]. Fig. 7(a) also shows that any of the two linear polarizations can dominate during a pulse, in contrast to Fig. 5(a) in which the $y-$polarization was dominant. The smaller value of f_m in Fig. 7(a) makes that both linearly polarized powers reach the spontaneous emission noise levels. In this way the polarization that is excited with larger power in each modulation period is mainly determined by the spontaneous emission noise events occuring just before the turn-on of the pulse.

Figs. 6(b) and 7(b) show the effect of increasing f_m to 10 GHz, a value above the relaxation oscillation frequency. This value has not been measured for $I_0 = 11.5$ mA but it can be estimated from its expression $f_R = (2\kappa\gamma(\mu - 1))^{1/2}/(2\pi)$ to obtain $f_R = 6.95$ GHz. Fig. 6(b) shows that the $y-$polarized optical frequency comb is recovered while the orthogonal comb has much less power. This can be explained by looking at Fig. 7(b): $y-$polarized power oscillates at 10 GHz but with a much smaller amplitude, 20, than in Fig. 5(a), 55. When the modulation frequency f_m is greater than the modulation bandwidth the GS regime is weakened, and the ON/OFF ratio for y-polarized pulses decreases from 3×10^3 for $f_m = 5$ GHz to 10 for $f_m = 10$ GHz. In Fig. 7(b) $y-$polarized ($x-$polarized) pulses are always well above (slightly above) the spontaneous emission noise level. Time traces of the carrier number are almost sinusoidal with a much smaller amplitude than in Fig. 5(b): they go from a minimum value of 0.89 N_{th} to a maximum value of $1.13N_{th}$. When f_m is increased from 3 GHz to 5 GHz the comb broadens. However, when f_m is greater than the modulation bandwith the GS regime is weakened and comb width decreases. The number of modes for the comb, $N_{\rm mod}$, with $m = 1.3$, constant, first increases then decreases when the RF frequency goes from 3 GHz ($N_{\rm mod} = 7$) to 5 GHz ($N_{\rm mod} = 9$) and then to 10 GHz ($N_{mod} = 3$). In this case the teeth depth increases when f_m increases from 3 GHz ($TD = 7$ dB) to 5 GHz ($TD = 30$ dB) and then to 10 GHz ($TD = 58$ dB). The broadest comb with a high teeth depth is obtained for an intermediate value of f_m, close to 5 GHz, in agreement with [7].

Figs. 6(c) and 7(c) show the effect of decreasing m with respect to the value considered in Fig. 5. Comparison between Figs. 6(c) and 4 shows that the frequency span of the $y-$polarized comb decreases and the teeth contrast increases when m decreases. Also the $x-$polarized comb has smaller power in Fig. 6(c). These observations can be understood when comparing Figs. 5(a) and 7(c). Oscillations of the $y-$polarized power in Fig. 7(c) are more sinusoidal, so the span in Fig. 6(c) is smaller. The minimum value of these oscillations is much larger when m is small resulting in a better phase coherence between pulses and larger teeth contrast. The fact that the $x-$polarized power is close to the noise level in Fig. 7(c) results in a low energy $x-$polarized comb. Results in Figs. 6(c) and 7(c) are qualitatively similar to those in Figs. 6(b) and 7(b). In both cases the GS regime is weakened. Figs. 6(d) and 7(d) show the effect of increasing m with respect to the value considered in Fig. 5. These results are qualitatively similar to those shown in Figs. 6(a) and 7(a). In both cases the GS regime enhances the power associated to the suppressed polarization mode. The number of modes for the comb with $f_m = 5$ GHz, constant, increases when the modulation index m goes from 0.5 ($N_{\rm mod} = 3$) to 1.3 ($N_{\rm mod} = 9$) and then to 2 ($N_{\rm mod} = 17$). However, the

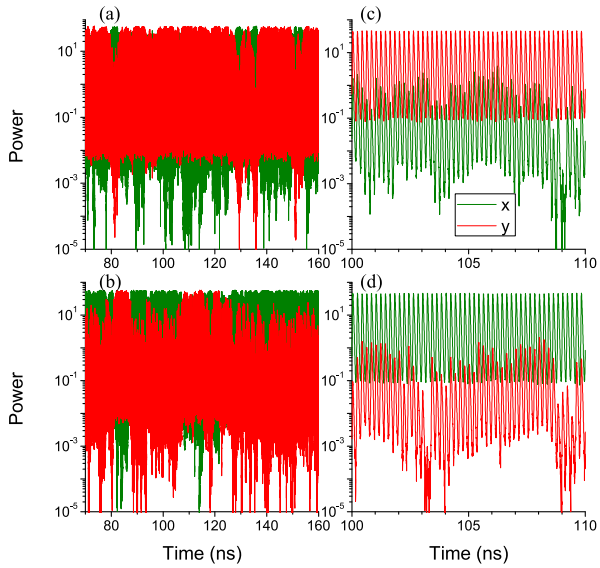

Fig. 8. Simulated time traces of the power of x (green line) and y-polarization (red line) modes. (a) $f_m = 5$ GHz, $m = 1.3$, $\gamma_a = 0.2$ ns^{-1} (b) $f_m = 5$ GHz, $m = 1.3$, $\gamma_a = 0$ (c) $f_m = 5$ GHz, $m = 1$, $\gamma_a = 0.15$ ns^{-1}, and (d) $f_m = 5$ GHz, $m = 1$, $\gamma_a = 0.15$ ns^{-1}. The bias current is $I_0 = 11.5$ mA.

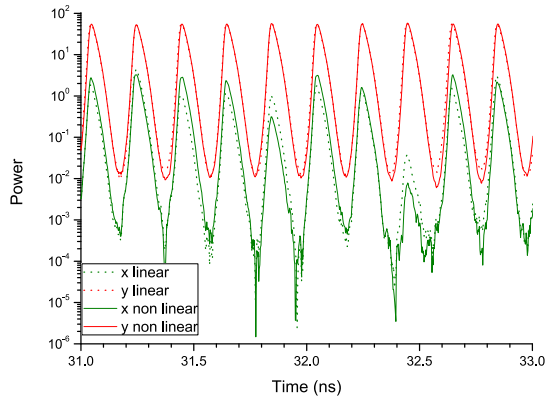

Fig. 9. Simulated time traces of the power of x (green line) and y-polarization (red line) modes. Traces obtained with the model with linear and nonlinear carrier recombination are plotted with dotted and solid lines, respectively. In this figure $f_m = 5$ GHz, $m = 1.3$, $\gamma_a = 1.4$ ns^{-1}, and $I_0 = 11.5$ mA.

comb almost disappears when $m = 2$ [see Fig. 6(d)]. When $f_m = 5$ GHz, the teeth depth decreases when m increases from 0.5 ($TD = 54$ dB) to 1.3 ($TD = 30$ dB) and then to 2 ($TD = 7$ dB). A trade-off between the number of modes and the teeth depth is obtained, and the characteristics of the comb are optimum for $m = 1.3$. This behavior shows that there is a value of m for which characteristics of both combs are optimum, in agreement with [7].

One way of obtaining a total optical comb with wider span is by enhancing the optical power associated to the suppressed polarization mode [7]. This can be done by using VCSELs with smaller values of the linear dichroism. Fig. 8 shows the effect of decreasing γ_a with respect to Fig. 5, on time traces of the power of both polarization modes. Fig. 8(a) shows that pulses of the suppressed $x-$polarization are excited over randomly distributed time windows of several ns duration when $\gamma_a = 0.2$ ns^{-1}. Excitation of $x-$polarized pulses is accompanied by suppression of $y-$polarized pulses. x-polarized frequency comb (not shown) is enhanced with respect to that in Fig. 4(c) because the maximum value of the x-polarized optical spectrum is just 4 dB smaller than the maximum corresponding to the $y-$polarization. Results corresponding to zero linear dichroism are shown in Fig. 8(b). Now, contrary to Fig. 8(a), $x-$polarized pulses are dominating with some randomly distributed bursts of $y-$polarized pulses. An optical comb with wider span is obtained because the maximum value of the x-polarized optical spectrum is 6 dB higher than the maximum corresponding to the $y-$polarization. Appearance of random bursts is due to the effect of spontaneous emission noise when the pulses have very small power. One way of trying to avoid this effect is by decreasing m in such a way that the minimum value of the power is above the noise level. Fig. 8(c) shows the power of both polarization modes when $m = 1$ and $\gamma_a = 0.15$ ns^{-1}. A regular and stable pulse train is observed for the $y-$polarized signal while $x-$polarized pulses are affected by noise as their minimum values are small. We have tried to get a situation in which both pulse trains are regular with no significant effect of spontaneous emission noise by decreasing γ_a. However, when $\gamma_a < 0.15$ ns^{-1} (not shown), x and y polarizations exchange their roles because $x-$polarized pulses become stable and regular while $y-$polarized pulses are dominated by noise. Another interesting feature can be observed in Fig. 8. Results corresponding to the same parameters of Fig. 8(c), but changing the random numerical sequence that simulates the spontaneous emission noise, are shown in Fig. 8(d). We observe that x and y polarizations exchange their roles with respect to Fig. 8(c). This means that there is bistability between two different solutions: one in which a stable and regular train of $y-$polarized pulses is observed (with suppressed x-polarization) and another in which the regular pulse train that is observed corresponds to the $x-$polarization (with suppressed y-polarization). So linear dichroism values can be found for which bistability between the two orthogonally polarized combs is observed.

V. Discussion and Conclusions

Section III has been devoted to extend the spin-flip model for including nonlinear carrier recombination. We now compare results obtained with the linear carrier recombination model with those obtained with the nonlinear one. We consider a situation for which a comb with good characteristics is obtained. Fig. 9 shows time traces of the power with the parameters of Fig. 5 compared to those obtained with the linear model, that is with (7)–(10). Both sets of results have been obtained using the same sequence of random numbers for the spontaneous emission noise simulation. Good agreement is found between both models for the power of the dominant mode: differences in the y-polarized maximum power are smaller than 4% in Fig. 9. Also good agreement is found for the carrier number (not shown): differences in the maximum value of N/N_{th} are smaller than 2%. However, Fig. 9 shows that differences in the x-polarized power can be very large. Good agreement between models with linear and nonlinear recombination was found in single polarization mode 850-nm VCSEL [16]. Our results indicate that including nonlinear carrier recombination is desirable in order to properly

describe the suppressed polarization of a VCSEL emitting in two polarization modes in the gain-switching regime.

To summarize, we have analyzed the polarization dynamics of a long-wavelength VCSEL subject to large amplitude gain switching modulation in order to get optical frequency combs. The analysis of the combs associated with the main and suppressed polarization modes has been done by using the spin-flip model. Extraction of the model parameters for a device used in previous optical frequency comb experiments has been performed in order to get a good theoretical description of comb formation in gain-switched VCSELs. An extension of the spin-flip model to include nonlinear carrier recombination has been developed and compared with the usual model with linear recombination. We have shown that two orthogonally polarized combs can combine to produce a wider overall optical comb. Our theoretical results give a similar dependence of combs on the amplitude and frequency of the modulation than that obtained in previous experiments. We have obtained an enhancement of the optical power associated to the suppressed polarization by decreasing the linear dichroism of the VCSEL. Finally, bistability between the two orthogonally polarized combs has been predicted. This bistability would permit switchings between orthogonally polarized frequency combs. These switchings could be induced for instance by optical injection of polarized optical pulses. This will be the subject of future work.

APPENDIX

The usual spin-flip model equations are given in (7)–(10) in which the meaning of the symbols is the following: D is the total population inversion ; n is the difference of the carriers associated with the spin-up and spin-down levels; and $E_{x,y}$ are the two linearly polarized electrical fields in the orthogonal x and y directions [22].

$$\begin{aligned}\frac{dE_x}{dt} =& -(\kappa+\gamma_a)E_x - i(\kappa\alpha+\gamma_p)E_x \\ &+ \kappa(1+i\alpha)(DE_x + inE_y) \\ &+ \left(\sqrt{\frac{R_+}{2}}\xi_+(t) + \sqrt{\frac{R_-}{2}}\xi_-(t)\right. \end{aligned} \tag{7}$$

$$\begin{aligned}\frac{dE_y}{dt} =& -(\kappa-\gamma_a)E_y - i(\kappa\alpha-\gamma_p)E_y \\ &+ \kappa(1+i\alpha)(DE_y - inE_x) \\ &+ i\left(\sqrt{\frac{R_-}{2}}\xi_-(t) - \sqrt{\frac{R_+}{2}}\xi_+(t)\right. \end{aligned} \tag{8}$$

$$\begin{aligned}\frac{dD}{dt} =& -\gamma[D(1+|E_x|^2+|E_y|^2) - \mu \\ &+ in(E_yE_x^* - E_xE_y^*)] \end{aligned} \tag{9}$$

$$\begin{aligned}\frac{dn}{dt} =& -\gamma_s n - \gamma[n(|E_x|^2+|E_y|^2) \\ &+ iD(E_yE_x^* - E_xE_y^*)] \end{aligned} \tag{10}$$

The bias current is given by the μ parameter [22]:

$$\mu = \frac{\tau_n}{\tau_e}\frac{\dfrac{I}{I_{th}} - 1}{1 - \dfrac{N_t}{N_{th}}} + 1 \tag{11}$$

where I, I_{th}, τ_n, τ_e, N_t and N_{th} have been defined in Section II. The other parameters of the SFM are the field decay rate, $\kappa = 1/(2\tau_p)$, the decay rate of D, $\gamma = 1/\tau_n$, the linewidth enhancemente factor, α, the linear dichroism, γ_a, the linear birefringence, γ_p, and the spin-flip relaxation rate, γ_s. Spontaneous emission is included in (7) and (8) by considering the following rates:

$$R_\pm = \beta_{SF}\gamma\left[(D \pm n) + \frac{G_N N_t}{2\kappa}\right. \tag{12}$$

where β_{SF} is the fraction of spontaneous emission photons coupled in the lasing mode and G_N is the differential gain [22]. β_{SF} can be obtained from the spontaneous emission rate at threshold by using $\beta_{SF} = R_{sp}^{th}\tau_n^2/(N_{th}\tau_p)$ [22]. Spontaneous emission noise is simulated by Gaussian white noises, $\xi_+(t)$ and $\xi_-(t)$ whose statistical properties are given in [32].

ACKNOWLEDGMENT

The authors thank I. Esquivias for useful comments. They would also like to thank Vertilas GmbH for facilitating the devices under investigation.

REFERENCES

[1] N. R. Newbury, "Searching for applications with a fine-tooth comb," *Nature Photon.*, vol. 5, no. 4, pp. 186–188, 2011.

[2] I. Coddington, N. Newbury, and W. Swann, "Dual-comb spectroscopy," *Optica*, vol. 3, no. 4, pp. 414–426, Apr. 2016. [Online]. Available: https://www.osapublishing.org/abstract.cfm?URI=optica-3-4-414.

[3] P. Martin-Mateos, M. Ruiz-Llata, J. Posada-Roman, and P. Acedo, "Dual-comb architecture for fast spectroscopic measurements and spectral characterization," *IEEE Photon. Technol. Lett.*, vol. 27, no. 12, pp. 1309–1312, Jun. 2015. [Online]. Available: http://ieeexplore.ieee.org/lpdocs/epic03/wrapper.htm?arnumber=7081780.

[4] A. R. Criado *et al.*, "Continuous-wave sub-THz photonic generation with ultra-narrow linewidth, ultra-high resolution, full frequency range coverage and high long-term frequency stability," *IEEE Trans. THz Sci. Technol.*, vol. 3, no. 4, pp. 461–471, Jul. 2013. [Online]. Available: http://ieeexplore.ieee.org/lpdocs/epic03/wrapper.htm?arnumber=6517547.

[5] J. He, F. Long, R. Deng, J. Shi, M. Dai, and L. Chen, "Flexible multiband OFDM ultra-wideband services based on optical frequency combs," *J. Opt. Commun. Netw.*, vol. 9, no. 5, pp. 393–400, May 2017. [Online]. Available: https://www.osapublishing.org/abstract.cfm?URI=jocn-9-5-393.

[6] T. P. McKenna, J. H. Kalkavage, M. D. Sharp, and T. R. Clark, "Wideband photonic compressive sampling system," *J. Lightw. Technol.*, vol. 34, no. 11, pp. 2848–2855, Jun. 2016. [Online]. Available: http://ieeexplore.ieee.org/lpdocs/epic03/wrapper.htm?arnumber=7414375.

[7] E. Prior, C. De Dios, M. Ortsiefer, P. Meissner, and P. Acedo, "Understanding VCSEL-based gain switching optical frequency combs: Experimental study of polarization dynamics," *J. Lightw. Technol.*, vol. 33, no. 22, pp. 4572–4579, Nov. 2015.

[8] E. Kapon and A. Sirbu, "Long-wavelength VCSELs: Power-efficient answer," *Nature Photon.*, vol. 3, pp. 27–29, Jan. 2009.

[9] E. Prior, C. de Dios, A. R. Criado, M. Ortsiefer, P. Meissner, and P. Acedo, "Expansion of VCSEL-based optical frequency combs in the sub-THz span: Comparison of non-linear techniques," *J. Lightw. Technol.*, vol. 34, no. 17, pp. 4135–4142, Sep. 2016. [Online]. Available: http://jlt.osa.org/abstract.cfm?URI=jlt-34-17-4135.

[10] F. Koyama, "Recent advances of VCSEL photonics," *J. Lightw. Technol.*, vol. 24, no. 12, pp. 4502–4513, Dec. 2006.
[11] R. Michalzik, *VCSELs: Fundamentals, Technology and Applications of Vertical-Cavity Surface-Emitting Lasers*, vol. 166. New York, NY, USA: Springer, 2012.
[12] M. San Miguel, Q. Feng, and J. V. Moloney, "Light-polarization dynamics in surface-emitting semiconductor lasers," *Phys. Rev. A*, vol. 52, no. 2, pp. 1728–1739, 1995.
[13] A. Valle, L. Pesquera, and K. Shore, "Polarization behavior of birefringent multitransverse mode vertical-cavity surface-emitting lasers," *IEEE Photon. Technol. Lett.*, vol. 9, no. 5, pp. 557–559, May 1997.
[14] K. Panajotov, B. Ryvkin, J. Danckaert, M. Peeters, H. Thienpont, and I. Veretennicoff, "Polarization switching in VCSEL's due to thermal lensing," *IEEE Photon. Technol. Lett.*, vol. 10, no. 1, pp. 6–8, Jan. 1998.
[15] B. Ryvkin *et al.*, "Effect of photon-energy-dependent loss and gain mechanisms on polarization switching in vertical-cavity surface-emitting lasers," *J. Opt. Soc. Amer. B*, vol. 16, no. 11, pp. 2106–2113, 1999.
[16] M. Bruensteiner and G. C. Papen, "Extraction of VCSEL rate-equation parameters for low-bias system simulation," *IEEE J. Select. Topics Quantum Electron.*, vol. 5, no. 3, pp. 487–494, May/Jun. 1999.
[17] A. Villafranca, J. Lasobras, J. A. Lazaro, and I. Garces, "Characterization of the main semiconductor laser static and dynamic working parameters from CW optical spectrum measurements," *IEEE J. Quantum Electron.*, vol. 43, no. 2, pp. 116–122, Feb. 2007.
[18] A. Consoli, J. Arias, J. Tijero, F. L. Hernández, and I. Esquivias, "Electrical characterization of long wavelength VCSELs with tunnel junction," *SPIE OPTO*, vol. 7952, 2011, Art. no. 79520C.
[19] A. Bacou, *Caractérisation et modélisation optoélectronique de VCSELs à grande longueur d'onde pour sous-ensembles optiques intégrés*, 2008. [Online]. Available: https://books.google.es/books?id=u8TSkQEACAAJ.
[20] A. Bacou *et al.*, "Electrical modeling of long-wavelength VCSELs for intrinsic parameters extraction," *IEEE J. Quantum Electron.*, vol. 46, no. 3, pp. 313–322, Mar. 2010.
[21] P. Pérez, A. Valle, I. Noriega, and L. Pesquera, "Measurement of the intrinsic parameters of single-mode VCSELs," *J. Lightw. Technol.*, vol. 32, no. 8, pp. 1601–1607, Apr. 2014.
[22] P. Pérez, A. Valle, and L. Pesquera, "Polarization-resolved characterization of long-wavelength vertical-cavity surface-emitting laser parameters," *J. Opt. Soc. Amer. B*, vol. 31, no. 11, pp. 2574–2580, 2014.
[23] V. M. Deshmukh, S. H. Lee, D. W. Kim, K. H. Kim, and M. H. Lee, "Experimental and numerical analysis on temporal dynamics of polarization switching in an injection-locked 1.55-μm wavelength VCSEL," *Opt. Express*, vol. 19, no. 18, pp. 16934–16949, Aug. 2011.
[24] R. Al-Seyab, K. Schires, A. Hurtado, I. D. Henning, and M. J. Adams, "Dynamics of VCSELs subject to optical injection of arbitrary polarization," *IEEE J. Select. Topics Quantum Electron.*, vol. 19, no. 4, Jul. 2013, Art. no. 1700512.
[25] Y. Ji-Yun, W. Zheng-Mao, L. Qing, C. Jian-Jun, Z. Zhu-Qiang, and X. Guang-Qiong, "Experimental determination of key parameters in the spin-flip model of 1550 nm vertical cavity surface-emitting laser," *Acta Phys. Sin.*, vol. 65, 2016, Art. no. 124203.
[26] S. P. Ó Dúill, P. M. Anandarajah, R. Zhou, and L. P. Barry, "Numerical investigation into the injection-locking phenomena of gain switched lasers for optical frequency comb generation," *Appl. Phys. Lett.*, vol. 106, no. 21, 2015, Art. no. 211105.
[27] G. P. Agrawal and N. K. Dutta, *Long Wavelength Semiconductor Lasers*. Dordrecht, The Netherlands: Springer, 1986.
[28] M. Ortsiefer, R. Shau, J. Rosskopf, and M. Amann, *Long-Wavelength InP-Based VCSELs*, vol. 6, H. Li and K. Iga, Eds. Berlin, Germany: Springer, 2003.
[29] D. Wiedenmann *et al.*, "Design and analysis of single-mode oxidized VCSELs for high-speed optical interconnects," *IEEE J. Select. Topics Quantum Electron.*, vol. 5, no. 3, pp. 503–511, May/Jun. 1999.
[30] N. Volet, "Optical mode control in long-wavelength vertical-cavity surface-emitting lasers," Ph.D. dissertation, Ecole polytechnique federale de Lausanne, Lausanne, Switzerland, 2014.
[31] J. Martin-Regalado, F. Prati, M. San Miguel, and N. Abraham, "Polarization properties of vertical-cavity surface-emitting lasers," *IEEE J. Quantum Electron.*, vol. 33, no. 5, pp. 765–783, May 1997.
[32] F. Denis-le Coarer *et al.*, "Injection locking and polarization switching bistability in a 1550 nm-VCSEL subject to parallel optical injection," *IEEE J. Select. Topics Quantum Electron.*, vol. 23, no. 6, Nov./Dec. 1997, Art. no. 1800910.
[33] S. M. Sze and K. K. Ng, *Physics of Semiconductor Devices*, 3rd ed. Hoboken, NJ, USA: Wiley, 2006.
[34] Y. R. Nosov, *Switching in Semiconductor Diodes*. New York, NY, USA: Plenum, 1995.
[35] A. Rosado, M. F. Vilera-Suarez, A. Perez-Serrano, J. M. G. Tijero, and I. Esquivias, "Characterization of optical pulses generated by gain switching a 1310 nm VCSEL," *X Reunión española de Optoelectrónica*, 2017. [Online]. Available: http://oa.upm.es/48760/1/OPTOEL2017Definitivo.pdf
[36] A. Mecozzi, A. Sapia, P. Spano, and G. P. Agrawal, "Transient multimode dynamics in nearly single-mode lasers," *IEEE J. Quantum Electron.*, vol. 27, no. 3, pp. 332–343, Mar. 1991.
[37] A. Valle, M. Sciamanna, and K. Panajotov, "Irregular pulsating polarization dynamics in gain-switched vertical-cavity surface-emitting lasers," *IEEE J. Quantum Electron.*, vol. 44, no. 2, pp. 136–143, Feb. 2008.

Ana Quirce received the Licenciada en Física (M.Sc.) and Ph.D. degrees in sciences, technologies, and computing in 2008 and 2012, respectively, from the University of Cantabria, Santander, Spain, where she was studying the dynamics of the polarization and transverse modes of vertical cavity surface-emitting lasers (VCSELs) subject to optical injection. She is currently a Post-Doctoral Fellow from the Research Foundation-Flanders with the Vrije Universiteit Brussel, Brussels, Belgium. Her current research interests include the areas of dynamics of VCSELs, optical injection effects in semiconductor lasers, optical feedback, optical frequency combs, and photonic integrated circuits.

Cristina de Dios received the Doctorate degree in 2010 for her work in ultrafast pulsed diode lasers and nonlinear pulse compression from the Universidad Carlos III de Madrid, Madrid, Spain. Currently, she is an Associate Professor with the Electronics Technology Department and a Member of the Optoelectronics and Laser Technology Group, Universidad Carlos III de Madrid. Her research interests include optical frequency comb generation techniques, pulsed semiconductor laser sources, nonlinear optical phenomena, and sub-terahertz and millimeter wave photonic signal synthesis and detection.

Angel Valle received the M.Sc. and Ph.D. degrees in physics from the Universidad de Cantabria, Santander, Spain, in 1988 and 1993, respectively. During 1994 and 1995, he was a Postdoctoral Fellow with the School of Electronic and Electrical Engineering, University of Bath, Bath, U.K. In 1996, he joined the Instituto de Física de Cantabria (CSIC-UC). Since 1998, he has been a Lecturer with the Departamento de Física Moderna, University of Cantabria. His research interests include the areas of vertical-cavity surface-emitting lasers, noise, and nonlinear dynamics of semiconductor lasers.

Luis Pesquera received the M.Sc. degree from the Universidad de Valladolid, Valladolid, Spain, and the Ph.D. degree from the Universidad de Cantabria, Santander, Spain, in 1974 and 1980, respectively, both in physics. He was a Postgraduate Fellow at the Universit de Paris VI, during 1977–1980. In 1980, he joined the Departamento de Fsica Moderna, Universidad de Cantabria. Since 1991, he has been a Professor of physics with the Universidad de Cantabria. In 1995, he joined the Instituto de Física de Cantabria (CSIC-UC). His research work started in the field of stochastic processes applied to physics and he has made contributions to the foundations of quantum physics, fluctuations in nuclear reactors, disordered systems, and laser physics. His current research interests include semiconductor laser dynamics, vertical-cavity surface-emitting lasers, and bio-inspired information processing.

Pablo Acedo (M'00) received the Doctorate (Hons.) degree from the Universidad Carlos III de Madrid, Leganes, Spain, in 2000. His doctoral work included the development of the first two-color laser system based on mid-IR sources for a stellarator fusion device (Stellarator TJ-II) and the first two-color Nd:YAG system for a fusion device (Tokamak C-Mod). In 2002, he was appointed an Assistant Professor by the Universidad Carlos III de Madrid. During the last years, he has been very active in the development of advanced spectroscopy techniques, mainly based on multiheterodyne architectures using dual-optical frequency combs, with applications in fields like gas spectroscopy, environmental applications, and, especially, in biomedical applications.